The GlueX Central Drift Chamber: Design and Performance

Y. Van Haarlem,[1] C. A. Meyer,[1] F. Barbosa,[2] B. Dey,[1] D. Lawrence,[2]
V. Razmyslovich,[2] E. Smith,[2] G. Visser,[3] T. Whitlatch,[2] G. Wilkin,[1] and B. Zihlmann[2]

[1]*Department of Physics, Carnegie Mellon University, Pittsburgh, Pennsylvania 15213, USA*
[2]*Thomas Jefferson National Accelerator Facility, Newport News, Virginia 23606, USA*
[3]*Department of Physics, Indiana University, Bloomington, Indiana 47405 USA*

Tests and studies concerning the design and performance of the GlueX Central Drift Chamber (CDC) are presented. A full-scale prototype was built to test and steer the mechanical and electronic design. Small scale prototypes were constructed to test for sagging and to do timing and resolution studies of the detector. These studies were used to choose the gas mixture and to program a Monte Carlo simulation that can predict the detector response in an external magnetic field. Particle identification and charge division possibilities were also investigated.

PACS numbers: 29.40.Cs; 29.40.Gx

I. INTRODUCTION

The GlueX Central Drift Chamber (CDC) is part of the GlueX experiment in Hall D at Jefferson Lab (Newport News, VA). This experiment aims to elucidate confinement in Quantum Chromo-dynamics, by searching for hybrid mesons that possess gluonic degrees of freedom and exotic quantum numbers [1], and arise from photo-production at 9 GeV [2, 3]. To achieve this goal, amplitude analysis on numerous exclusive reactions must be carried out to determine the quantum numbers of produced exotic mesons, which decay into photons and charged particles. Clearly, an overall hermetic detector with adequate resolution is essential, and the CDC is a crucial subsystem.

Straw tubes are a well-established technology [4–30] that has long been recognized as an alternative to multi-wire tracking chambers. Due to their cylindrical geometry, straw tubes can have very low mass, which reduces multiple scattering of charged particles. Individual wire breakage does not affect neighboring wires because each straw is self-contained. Another advantage of straw tubes is that they can support their own wire-tension and in this way the end-plates (plates that hold the straws) can be made much thinner compared to a conventional wire chamber, which also reduces multiple scattering.

The CDC will consist of 3500, 1.5 m long, straw tubes. The straws are mounted in 28 layers: 12 axial and 16 stereo; the placement of the straws is chosen to minimize tracking ambiguities. The inner and outer diameters of the chamber are 20 and 120 cm respectively. Gas plenums are constructed outside each end-plate. These plenums allow gas to be distributed to all the straws at the same time instead of feeding gas to straws individually. High voltage distribution boards and pre-amplifiers are mounted on the upstream gas-plenum, outside the gas volume. The output signals of the pre-amplifiers travel over a 20 m long cable to readout-electronics in VME crates.

The CDC will be operated inside a solenoid that generates a magnetic field of 2.24 T. The goal for position reso-
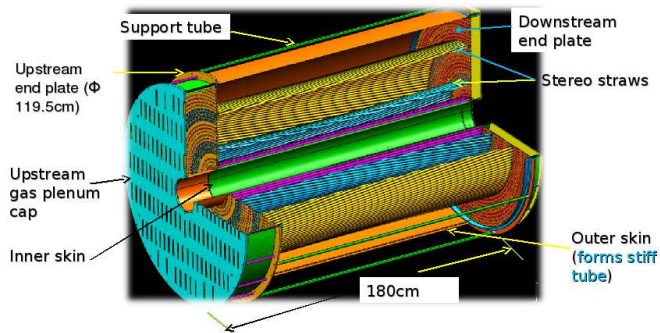

FIG. 1: Drawing of the final CDC design.

lution is 150 μm transverse to the wire and 1.5 mm along the axis of the chamber. Full tracking will be achieved using both the CDC and the Forward Drift Chambers, which are located directly downstream from the CDC. The target will be located 25 cm upstream from the center of the CDC. The polar angular coverage is between 6 and 165°. This detector is designed to enable measurements in energy loss dE/dx needed for particle identification of pions, kaons, and protons with momenta lower than 450 MeV [1]. A drawing of the final CDC design is shown in Fig. 1.

First the straw tube design will be presented, with tests concerning sagging and radiation damage. Then the electronics and gas system is introduced, followed by studies to characterize the detector. These studies are used to construct a Monte Carlo simulation that describes the detector performance, followed by timing and resolution studies. The possibility of obtaining particle identification (PID) by measuring the energy loss of the particles in the straw volume is investigated using the Monte Carlo simulation. Possible improvement of position resolution along the wire by application of charge division is investigated, followed by final remarks and conclusions.

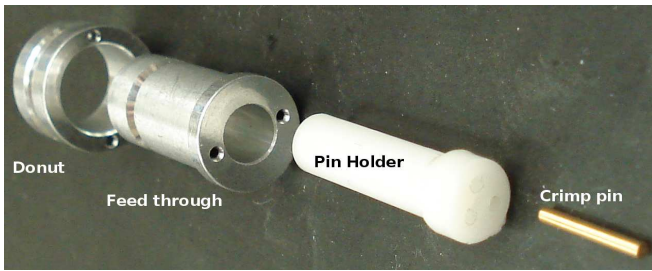---

[1] The speed of light (c) is set to one in this note.

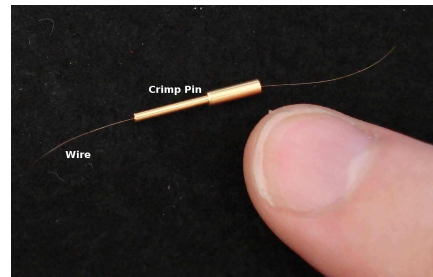FIG. 2: Picture showing the straw end assembly (upstream end). See text for more details.

FIG. 3: Picture showing the wire used in the straw tubes together with a crimp pin (not the final design) that holds the wire in place.

II.   STRAW TUBE DESIGN

The straws that will be used are 150 cm long, with an inner diameter of 1.6 cm. Fig. 2 shows a picture of the straw tube end assembly at the upstream end. The wires are held in place using a metallic crimp pin. The pin is inserted in a Noryl holder that has three extra holes to allow for gas flow into the straw. The pin holder is inserted into a feed-through that is glued into the end-plate and into a donut. The donut is glued to the inside of the straw. At the upstream end of the chamber, the donut and feed-through are made of aluminum to provide an electrical ground connection between the end plate and the aluminum on the inside of the straw tube. At the downstream end, the donuts are made of Noryl to minimize the material along the particle tracks. Detailed specifications of the donut and feed-through can be found in [31][2]. In following sections details about the wire and straws will be provided and the results of a sag and irradiation test are discussed. It is important that the straws do not sag because that causes the uniformity of the electric field to vanish. The irradiation test was performed to test the robustness of the aluminum layer inside the straw. If that layer gets damaged, it can cause noise or even a dead straw.

A.   Sense wire

The sense wire material used in all tests and in the final design is gold plated tungsten wire manufactured by California Fine Wire[3]. The wire has a total diameter of 20 μm. The tensile strength of this wire is 21,000 kg/cm^2. The wires in all test chambers are tensioned to 37 g, which is about half the yield point of 75 g.
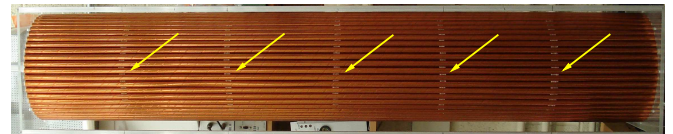

FIG. 4: Picture of a prototype used for sagging test. A full circle of 1.5 m long straws was put in place and spot-glued together. Rings of glue spots are visible and indicated by yellow arrows.

B.   Straw

A straw consists of several layers of thin (20-30 μm) mylar or kapton with a thin aluminum layer on the innermost one, which acts as a cathode. The straw tubes used for the CDC are 1.5 m long and have an inner radius of about 7.8 mm and a wall thickness of about 100 μm.

Individual straws of this length sag by several mm under their own weight. This sag can significantly distort the drift properties of the electrons. In order to avoid this, straws are mounted in layers of circles and spot glued together to prevent the sagging. This is tested by constructing a ring (diameter 25 cm) of 1.5 m long straws that are spot-glued together. The setup is shown in Fig. 4. No measurable sagging is observed.

C.   Radiation exposure test

1.   Prototype

To verify the stability and integrity of the aluminum layer at the inside surface of the straw an irradiation test was performed on a small scale prototype chamber with four different, 30 cm long, straw types. This prototype was fully operational and could be read out if desired. The 4 straw types that were put into the testing prototype were a kapton straw with a <1 μm vapor-deposited aluminum layer on the inside produced by Stone Indus-

———

[2] GlueX documents mentioned in this note are public and can be found on http://argus.phys.uregina.ca/cgi-bin/public/DocDB/DocumentDatabase

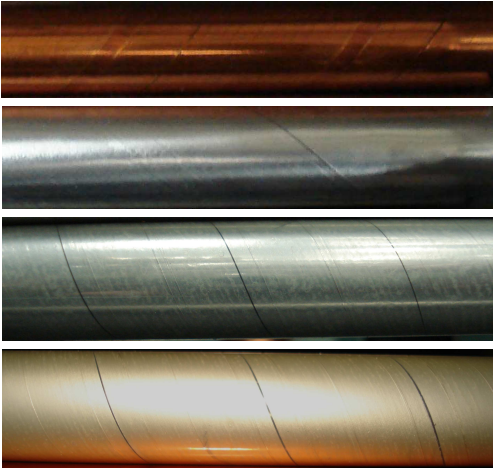[3] California Fine Wire, P.O. Box 446, Grover Beach, CA 93483-0446, http://www.calfinewire.com

FIG. 5: Picture of the different straw types that were irradiated (not to scale). From top to bottom: Stone Industrial kapton straw with < 5 μm thick aluminum layer inside, Euclid Spiral Paper Tube Corp. mylar straw with an aluminum layer (unknown thickness) inside, Lamina mylar straw with a 0.03 μm aluminum layer inside, and Lamina mylar tube with a 12 μm aluminum layer inside.

trial[4] (referred to as Stone-kapton), a mylar straw with a <1 μm vapor-deposited aluminum layer on the inside produced by Euclid Spiral Paper Tube Corporation[5] (referred to as Euclid-mylar), and two straws consisting of 4 layers of 25 μm thick mylar produced by Lamina Dielectrics Ltd[6]: one with 0.03 μm vapor-deposited aluminum on the inside mylar layer (referred to as Lamina-thin) and one with a 12 μm thick aluminum foil glued on the inside mylar layer (referred to as Lamina-thick). There were only two straw candidates considered for the final design: the Lamina-thick and Lamina-thin straw because the Euclid-mylar straw is not robust enough and the Stone-kapton straw is not as cost-effective as mylar. A picture of the four different straw types is shown in Fig. 5. The straw type of preference is the Lamina-thin one because this straw has the least amount of material (smallest wall thickness) which means a minimal probability of photon conversion and multiple scattering of particles passing through the CDC.

2. Radiation dose

The source used for irradiation was a $3.7 \cdot 10^6$ Bq ^{90}Sr source. The source was collimated and a length of about

—————

4 Stone Industrial, 9207 51st Ave., College Park, MD 20740-1910, http://www.stoneindustrial.com
5 Euclid Spiral Paper Tube Corporation, 339 Mill Street, P.O. Box 458, Apple Creek, Ohio 44606, http://www.euclidspiral.com
6 Lamina Dielectrics Ltd, Daux Road Billingshurst, West Sussex RH14 9SJ, United Kingdom, http://www.laminadielectrics.com

1 cm of the straw was irradiated. The accumulated dose per straw is shown in Table I, expressed in C/cm, which is the charge seen by the wire per cm. All the doses are

Straw type	Dose [C/cm]
Stone-kapton	0.009
Euclid-mylar	0.004
Lamina-thin	0.010
Lamina-thick	0.004

TABLE I: Received doses of the irradiated straws.

well below 1 C/cm which can rule out traditional ageing effects (like the Malter effect) on the straws. These doses are equivalent to about 44 years of running in the GlueX experiment for the most heavily exposed straws. During irradiation the gas mixture flowing through the prototype was an argon-CO_2 (90%-10% by volume) mixture and the wire was set at the nominal operating voltage of 1450 V. The straws were grounded. Irradiated straws were later compared to unused (reference) straws that were neither irradiated nor used in a chamber with gas or High Voltage (HV). In the following section the results are discussed. In general, all straws were still operational after irradiation with no performance loss. More details concerning this test can be found in Ref. [32].

3. Lamina-thin

An unused reference Lamina-thin straw was compared, using an electron microscope, with a piece that has been irradiated. Pictures at low scale are shown in Fig. 6. At this scale black "lines" can be seen on both sample surfaces. It is believed that they are an artifact of manufacturing. Pictures of a pristine straw taken with an optical microscope are shown in Fig. 7. One can see that the black "lines" mentioned before are in fact scratches partially or completely through the aluminum layer.

A difference observed between the pristine and irradiated straw are the dark gray areas (one area is indicated with a yellow ellipse in Fig. 6) on the irradiated straw which are not visible on the reference straw. In Fig. 8, at a factor of 20 higher resolution, one can see that the irradiated straw shows black pits and that the dark gray areas indicated in Fig. 6 are in fact a different size and concentration of those black pits (as can be seen in the center of Fig. 8). The origin of the pits remains unclear but they have a relative higher amount of oxygen present than the surrounding area. The relative amount of atoms can be determined by doing an analysis of X-rays coming from the straw when under the electron microscope, three lines with different intensity are always observed: aluminum, oxygen, and carbon. The pits are also observed in straw parts that were used in the radiation exposure test but were located far away (20 cm) from the Sr-source and in a Stone-kapton straw that was used for three years but then the effect was less intense and no difference in
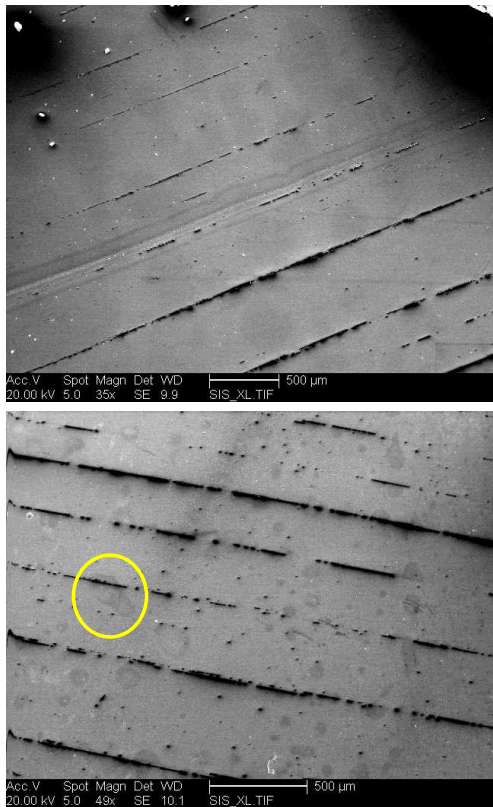
FIG. 6: Comparison of the aluminum surfaces between a pristine Lamina-thin straw (top) and one that was irradiated (bottom). The scale of 500 μm is indicated at the bottom of each picture. A dark gray area, with a black "line" going through it, is emphasized by the yellow ellipse.

oxygen content could be measured. This suggests that the spots are caused by a chemical reaction triggered by radiation and the presence of an electric field.

4. Lamina-thick

A piece of a pristine Lamina-thick straw is compared, using an electron microscope, to a piece that was irradiated. The result at low resolution is shown in Fig. 9. Both straw surfaces look very smooth compared to the same pictures taken of the Lamina-thin straw. On this scale one can see that there is no substantial difference between the two. Also at higher magnification no differences can be seen (Fig. 10). The white dots are little pieces of pure iron, probably stemming from fabrication. The difference with the previous straw (Lamina-thin) is, according to the manufacturer, that there is an aluminum foil being glued to a mylar sheet instead of being vapor-deposited. There were no holes or scratches observed that go through the aluminum layer when looking at it with an optical microscope with a light source mounted underneath the straw.

FIG. 7: Picture taken of a pristine Lamina-thin straw with an optical microscope. The upper picture shows the straw sample lighted from the top side and a scratch is visible; the red line in the lower right corner indicates 25 μm. The lower picture shows the straw sample with a light source below it, the white lines and dots are holes or scratches through the aluminum layer.

5. Gold plated tungsten wire

The 20 μm diameter gold plated tungsten wire was also examined before and after the radiation test. A comparison is shown in Fig. 11. As the radiation doses are low (much lower than 1 C/cm) no radiation damage is to be expected. Indeed there is no obvious difference observed between the irradiated and the pristine wire.

D. Straw choice

The straw type choice is not straightforward as the Lamina-thin one has the least amount of material but shows scratches, holes and some unexpected behavior after radiation. However, the straw was still operational after radiation with no performance loss. The tests performed do not give any information of how this will evolve over time. The Lamina-thick straw shows a very stable behavior but the aluminum layer is too thick. The straw of choice will be the Lamina-thin one but with a thicker vapor-deposited aluminum layer, probably between 0.5 and 1 μm. They will be checked before usage. The total wall thickness of this straw will be between 100 and
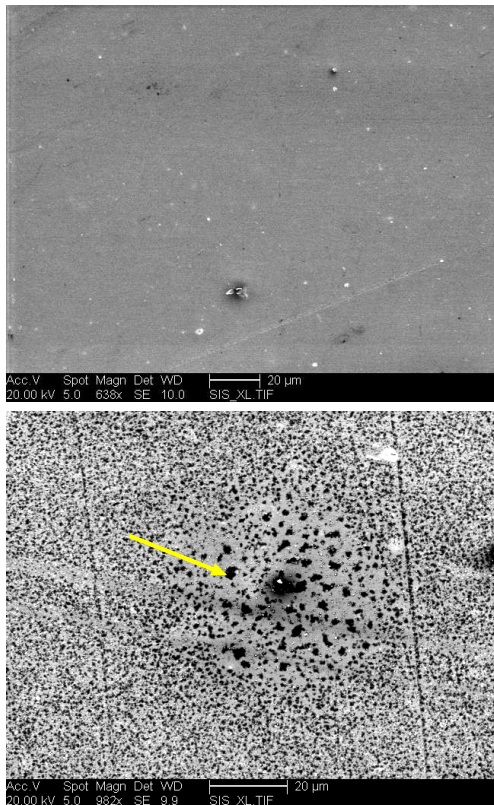
FIG. 8: Comparison of the aluminum surfaces between a pristine Lamina-thin straw (top) and one that was irradiated (bottom) at a scale of 20 μm, as indicated at the bottom of the pictures. The center of the picture on the bottom is a further magnification of one of the dark gray areas as seen in Fig. 6 (bottom). The yellow arrow points to a typical black pit.
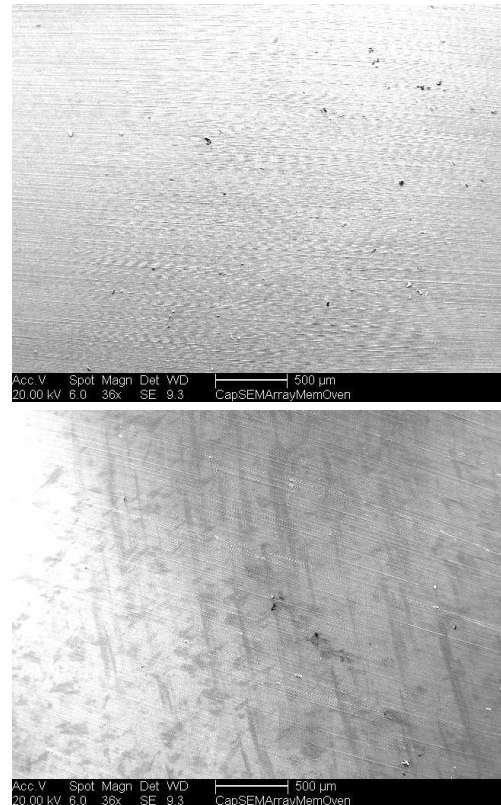

FIG. 9: Comparison of the aluminum surfaces between a pristine Lamina-thick straw (top) and the one that was irradiated (bottom) at a scale of 500 μm as indicated at the bottom of the pictures.

101 μm depending on the thickness of the inner aluminum layer. The inner radius of the straw is 7.8 mm.

E. Straw placement

The straws will be arranged in 28 layers. From the inside out: two double (a layer followed by a close packed layer) axial layers, followed by two sets of: two double +6° stereo layers, two double -6° degree layers and two double axial layers. A drawing showing the placement of the straws is shown in Fig. 12. This setup has been carefully chosen after extensive Monte Carlo (MC) simulations in order to minimize tracking ambiguities [33]. The innermost layer of straws is at a radius of 9 cm and the outermost layer at a radius of 59.75 cm.

III. GAS SYSTEM AND FLOW

The gas mixture that is intended to be used is a mixture of argon and CO_2. Flammable gas components are avoided for safety reasons. The gas system to flow the gas mixture through the prototypes consists of two MKS Instruments[7] Mass-Flo controllers one for argon and one for CO_2 gas. They are read-out and controlled by a MKS Instruments Inc. Multigas controller. The gas is mixed in a buffer volume of 34.4 l before being fed into the downstream end plenum of the detector. On the upstream and downstream end of the CDC a gas plenum is constructed where all the straws end. This construction allows to have one gas inlet into the downstream gas plenum to feed gas to all the straws and one gas outlet on the upstream end plenum to extract the gas from all the straws. In the GlueX experiment the gas flows as follows: gas will flow into the downstream end plenum through 6 plastic tubes. Gas then flows through the straws into the upstream end plenum where it can flow through 6 holes in the upstream end plate into the volume between straws. This volume will be made gas tight. Gas is extracted from this volume though 3 plastic tubes going through the upstream end plenum and end plate. The pressure is
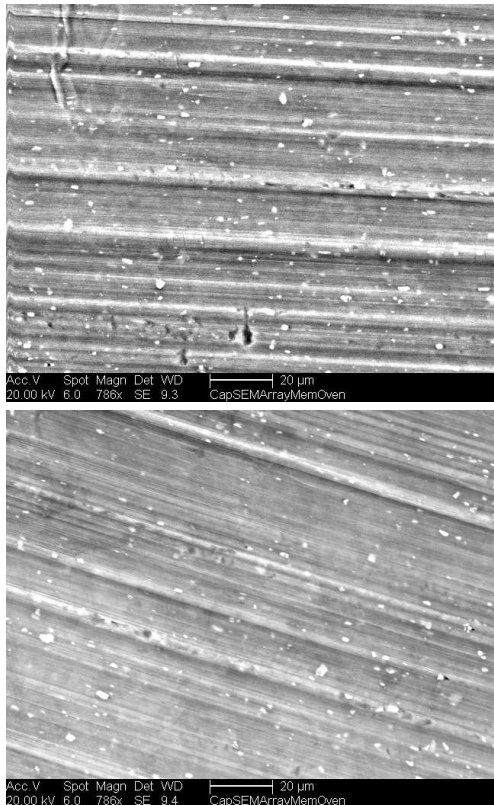
———

FIG. 10: Comparison of the aluminum surfaces between a pristine Lamina-thick straw (top) and the one that was irradiated (bottom) at a scale of 20 μm as indicated at the bottom of the pictures.

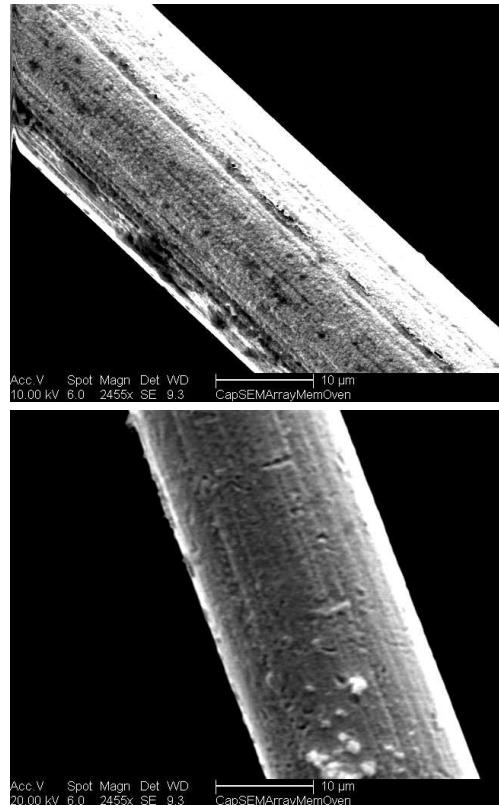FIG. 11: Comparison between a pristine wire (top) and one that was irradiated (bottom) at a scale of 10 μm as indicated at the bottom of the pictures.

slightly above 1 atm and the gas flow in the prototype is a few detector volumes per hour. About three volume exchanges per day are anticipated for the gas system in the GlueX detector [34]. The gas temperature and pressure will be monitored.

IV. ELECTRONICS

The inside aluminum surfaces of the straw tubes are connected to ground while the wires are held at a voltage between 1400 and 2300 V (depending on the gas mixture). The wires are connected to cables that run through the end plenum to HV-boards [35] located outside of the gas volume. These printed circuit boards distribute high voltage to the wires and decouple the signal from the high voltage line (it also protects against high currents and filters high frequency noise on the high voltage line). This board hosts an ASIC charge-sensitive pre-amplifier [36]. The charge-amplified signal of the current prototypes is
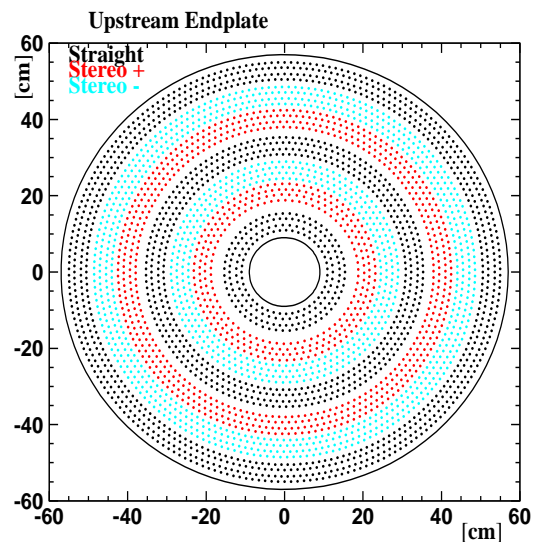

FIG. 12: Drawing of the front view of straw position in the upstream end plate. Black dots represent axial straws, red and blue dots represent straws with a stereo angle of plus and minus 6° respectively.
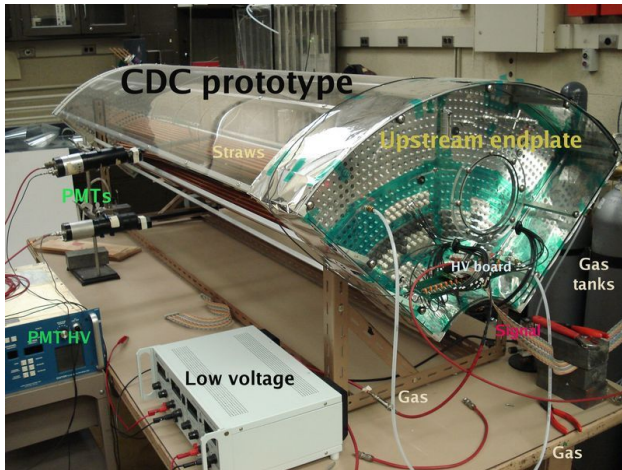
FIG. 13: Picture showing a one quarter section of a full-length prototype of the CDC.

shaped by a shaper board [37] and readout by Struck[8] SIS3320 12 bit flash ADCs running with a 125 MHz external clock. They are run at 125 MHz (they can run up to 200 MHz) because in the GlueX experiment the shaper and the flash ADC will be combined into one VME module [38] that will run with an 125 MHz external clock. This module is being designed and tested at Jefferson Lab.

V. PROTOTYPES

Three different prototypes have been constructed. First, a full-length prototype of one quarter of the final CDC was built with two different straw types: Stone-kapton and Euclid-mylar straws. The straws are 2 m long (in the final design the straws will be 1.5 m long). A picture of this prototype is shown in Fig. 13. This prototype was mainly constructed to confirm the feasibility of the design and to optimize details in the construction of the detector. It turned out that the Euclid-mylar straws can be easily deformed and the Stone-kapton straws not. Tests were also done to compare the options of placing the electronics either inside or outside the gas plenum. Both configurations could be implemented in the experiment with acceptable distance between the wire and the pre-amplifier so it was decided to locate the electronics outside the gas plenum to facilitate access. Operating this prototype revealed the necessity for generous solid ground connection between the end-plate that connects to the aluminum surfaces of the straws and the pre-amplifier to minimize electronic noise.

Design problems identified in the full-length prototype

----

[8] Struck Innovative Systeme GmbH, Harksheider Str. 102A, 22399 Hamburg, Germany, http://www.struck.de
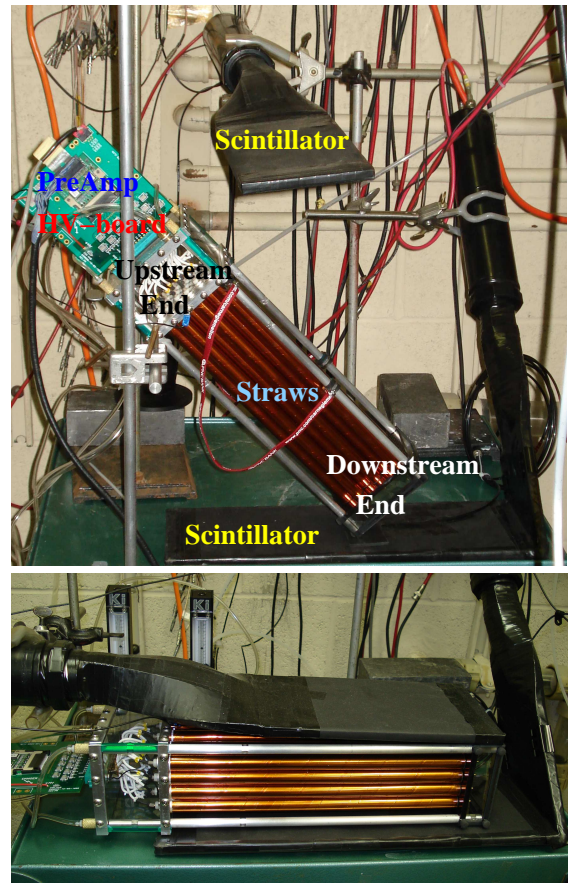

FIG. 14: Pictures showing a small scale prototype of the CDC with a scintillator above and below (for cosmic ray triggering) the prototype. Above the prototype is tilted and the different parts are labeled, at the bottom side the prototype is positioned horizontal with a scintillator mounted above and below the chamber.

are corrected and improvements are implemented in the small prototype (shown in Fig. 14). The small prototype has 24 straws that are 30 cm long with two gas end-plenums. The electronics are mounted outside the "up-stream" gas plenum. The straws are in a close packed configuration as shown in Fig. 15 but only 14 of the 24 channels are connected due to limited availability of readout channels.

VI. CHARACTERIZING THE DETECTOR

The following sections describe measurements to determine characteristics which must be determined before more complicated studies can be performed. First, the detector response to a ^{55}Fe source is studied. Then, gas gains are calculated.
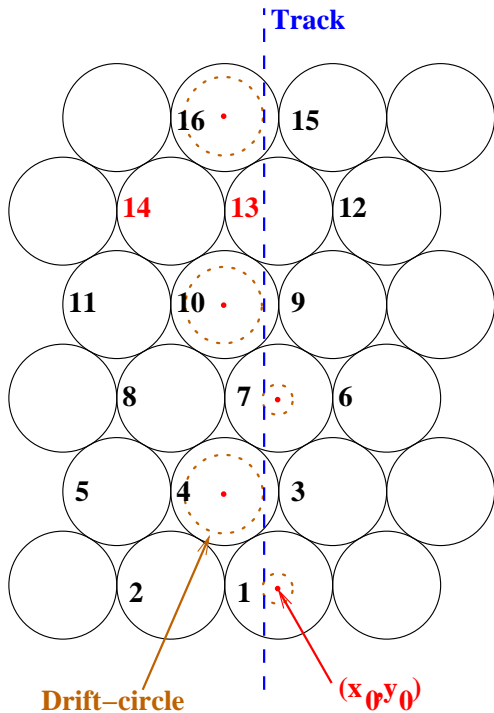
FIG. 15: View of the cross section of the close packed straw arrangement of the small scale prototype. The channels 13 and 14 indicate broken channels in the readout electronics while unnumbered straws are not connected to any readout electronics. A possible track and drift-circles illustrate the tracking mechanism in the x-y plane, see text for more details.

A. ^{55}Fe energy spectra

Fig. 16 shows the detector response to a ^{55}Fe source using several different argon-CO_2 gas mixtures. One can identify a large peak (the argon-peak) at the high end of the energy spectrum. This is the 5.966 keV peak where the X-ray (from the ^{55}Fe source) is being absorbed by the argon atom and two electrons are freed. The second peak, at lower energy, is the argon-escape peak (the excited argon atom emits an X-ray that has a high probability of escape) and has an energy of about 2.9 keV. The energy resolution degrades with increasing CO_2 admixture as can be seen by the increasing width of the argon peak. This behavior can be parameterized with a linear function:

$$\sigma_E = 815 + 27.5 \cdot x_{CO_2}, \qquad (1)$$

with σ_E the width of the argon-peak and x_{CO_2} the amount in % of CO_2 in the argon-CO_2 gas mixture.

B. Monte Carlo simulation

The MC simulation of the small scale prototype is written using GARFIELD [39]. In this simulation a track is
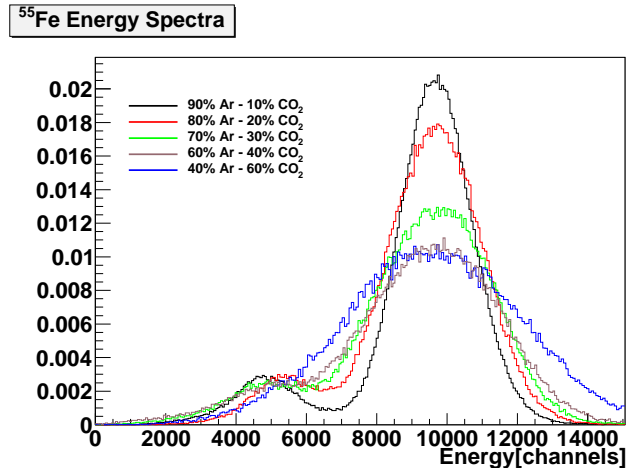

FIG. 16: Detector response to the ^{55}Fe source recorded by the flash ADC for different argon-CO_2 gas mixtures. The spectra are corrected for slight gas gain differences and are normalized to each other.

generated by two points, one above and one below the detector. Those uniformly generated random points are connected with a straight line and it is determined which straws are intersected by a track. The distance from the track to the wire in the straws that are hit is then passed to GARFIELD which returns output currents as a function of time. Those currents are convoluted with a response function of the electronics chain up to the flash ADC. This function is obtained experimentally by injecting a fast step function signal from a function generator into the readout chain and sampled at its output using an oscilloscope. The amplitude of this signal is sampled at a rate of 125 MHz, the same frequency as the flash ADC, and written to disk in the same format as the data acquisition system. In this way the same code can be used to analyze real data as well as simulated data and the two can be directly compared. An advantage of this method is that it can include the effects of the magnetic field on the drift chamber response using GARFIELD but still work with straight tracks. GARFIELD will add drift to the electrons' path as if there was a magnetic field present. In this way, straight line tracking can still be used.

VII. GAS CHOICE

In the following section, more complex measurements are described that directly influence the choice of the operating gas mixture. First, the working voltage for each gas mixture is determined. This is followed by gas gain, timing, and resolution studies. Scintillators are placed above and below the prototype, as shown in Fig. 14. Typically, one chooses a noble gas (argon) and a quencher gas (CO_2). The quencher absorbs photons originating from excited noble gas atoms. In general these photons have an energy large enough to free electrons from the alu-
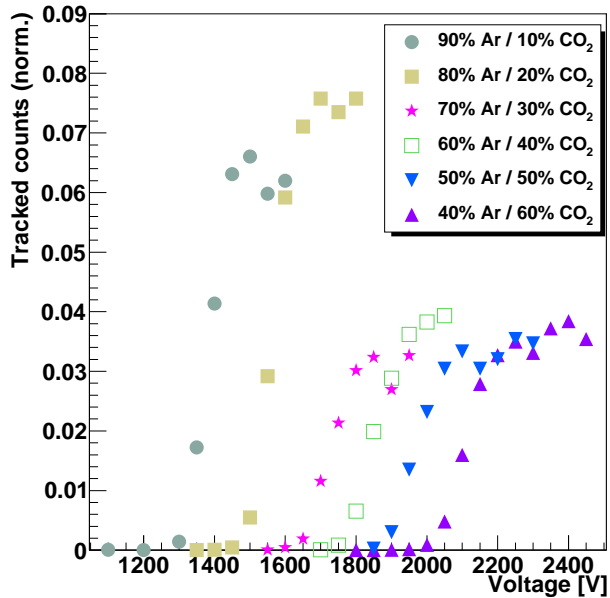
FIG. 17: Cosmic ray detection efficiency as a function of high voltage for several argon/CO_2 gas mixtures.

Gas [% Argon - % CO_2]	Working voltage [V]
90-10	1450
80-20	1700
70-30	1800
60-40	1950
50-50	2100
40-60	2250

TABLE II: Operating voltages for several gas mixtures.

of gas mixture. The detector response to ^{55}Fe spectra can be simulated and fit to real data. The only free parameter is the gas gain. Table III shows gas gain for different applied voltages and gas mixtures, measured at voltages lying on the plateau. Gas gain between 10^5 and 10^6 is observed.

Gas [% Argon - % CO_2]	Voltage [V]	Gas gain [10^5]
90-10	1450	1.5
80-20	1700	1.4
70-30	1750	1.6
70-30	1800	1.7
60-40	1900	1.7
50-50	2100	3.1
40-60	2150	1.5

TABLE III: Gas gains for different gas mixtures and high voltage settings.

minum inside the straw, this can cause sparks and limits the gas gain.

A. Operating voltage

Cosmic ray data were taken at different high voltage settings and gas mixtures. Tracks were reconstructed to count the number of cosmic rays that passed through a given straw. That number is normalized to the total number of cosmic triggers. The results for different argon-CO_2 mixtures as a function of operating voltage are shown in Fig. 17. One can clearly see that the onset of the plateau shifts to lower voltages as the argon concentration in the gas mixture increases. The nominal operating voltage for a given gas mixture is chosen to be slightly above the onset of the plateau to be insensitive to small voltage variations but minimize the dark current at the same time. The different plateau heights for the different gas mixtures are due to the fact that the parameters for drift time (see section VII C) and time-to-distance relations (see section VII D), which are used by the tracking algorithm, are not optimized for each gas mixture separately. The working voltages for the different gas mixtures are shown in Table II. The width and position of the pedestal was also studied as a function of bias voltage and no significant changes were observed.

B. Gas gain

The MC simulation described in section VI B can be used to determine the detector gas gain as a function

C. Drift times

An important input parameter for the tracking algorithm is the time difference between the initial ionization and the arrival time of the first electron, referred to as drift time. This is the time which the ionization electron generated closest to the wire needs to drift to the wire. The drift time is obtained from the flash ADC instead of a time-to-digital converter. The flash ADC samples the signal at a rate of 125 MHz, recording 512 time samples of 8 ns, where each time sample contains the measured signal amplitude digitized in a 12 bit word (the trigger prompting readout and storage of the ADC data is timed to ensure that the signal data are placed well within this 4096 ns time window). The rising edge of the signal is located as follows: A signal threshold is calculated from the recorded pedestal values as pedestal mean plus 10 times pedestal width, and the first time sample where the signal exceeds this threshold is then found and used as a starting point to determine the rising edge. The algorithm scans successively earlier time samples until a local ADC minimum is reached, and successively later samples until a local ADC maximum is reached. These two samples are then taken as the start and the finish of the leading edge. The time samples forming part of the leading edge are then examined to enable a reduced
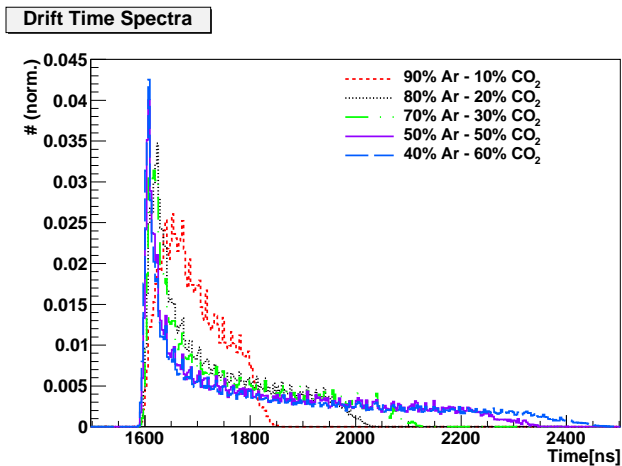
FIG. 18: Drift time spectra for different argon-CO_2 gas mixtures.

number of time samples to be selected for use with the DCOG method. Selection is based on the the difference in ADC value between each time sample and those of its neighbors. For time sample i, d_i is the increase in ADC value, ADC_i, from that of the previous time sample:

$$d_i = ADC_i - ADC_{i-1}. \qquad (2)$$

The maximum difference (d_{max}) is the maximum value of d_i and is located (in time) in the middle of the leading edge. Only time samples that have d_i larger than $f \cdot d_{max}$ are accepted as part of the leading edge and passed to the DCOG method. It was empirically found that $f = 0.3$ produces the best tracking resolutions. If it turns out that this algorithm is too complex to be programmed in the flash ADC, f will be set to zero. This will result in a position resolution that is about 8 μm worse compared to $f = 0.3$.

Using only the selected samples of the leading edge the extracted drift time (t_d) equals:

$$t_d = \frac{\sum_{i=2}^{n} d_i \cdot t_i}{\sum_{i=2}^{n} d_i}, \qquad (3)$$

with n the number of samples of the leading edge that are used and t_i is the time stamp of time-sample i. There are other methods to extract the drift time, such as the First Electron Method (FEL) where a line if fit to the leading edge, but using the DCOG method resulted in the best resolution. Drift time histograms for different gas mixtures are shown in Fig. 18. One can observe clear differences between gas mixtures. The more CO_2 is added, the longer the drift time becomes. The "rising edge" of the drift time histogram is fit with a linear function to extract the lowest possible value for the drift time t_0, that is when the ionization-electron is generated very close to the wire. The actual drift time is then $t_d - t_0$.

The upper limit for the drift time corresponds to the drift distance between the straw wall and the wire. This time should be kept below 1 μs in order to minimize pile-up. In Table IV the maximum drift times are listed for the various gas mixtures that were tested. The maximum drift time increases with increasing CO_2 content and reaches 900 ns for the 40%-60% argon-CO_2 gas mixture without the presence of an external magnetic field. See section VII D 4 for a discussion for the response in the magnetic field environment of the experiment.

| Gas | Maximum drift time [ns] | |
[% Argon - % CO_2]	B = 0 T	B = 2.24 T
90-10	250	N/A
80-20	420	N/A
70-30	480	620
60-40	590	670
50-50	750	790
40-60	900	920

TABLE IV: List of the maximum drift time for the gas mixtures that were tested without an external magnetic field and simulated with an external magnetic field (see section VII D 4).

D. Position resolution

Once the actual drift time ($t_d - t_0$) is extracted, it is converted into a distance from the wire (radius). This conversion is performed using time-to-distance tables that are calculated using GARFIELD. In Fig. 19 this relationship is shown for two gas mixtures with no external magnetic field applied. Once drift radii are extracted, they can be used in the track finding/fitting algorithm and resolutions can be calculated. Tracks are defined in the plane perpendicular to the wires. An illustration of how the tracking works is shown in Fig. 15. The brown drift-circles are circles defined by the extracted drift radii. If there are more than three hits, a track can be fit: this is shown as the blue line.

1. Track finding

When a cosmic ray passes through the detector, it can traverse through multiple straws. An electrical signal is induced on the wire in each straw which the cosmic ray passed through. From timing characteristics of this signal the distance of closest approach can be reconstructed (hit-radius). When 3 or more hit-radii are reconstructed in an event, a track finding algorithm is applied. Every combination of two hit-radii is taken to provide four possible tracks by tangent lines connecting the two circles defined by the two hit-radii. These trajectories are then used to search other straws with hit-radii within a 4 mm window of these track candidates. The track with the most hits or the lowest χ^2/dof (if the number of hits is
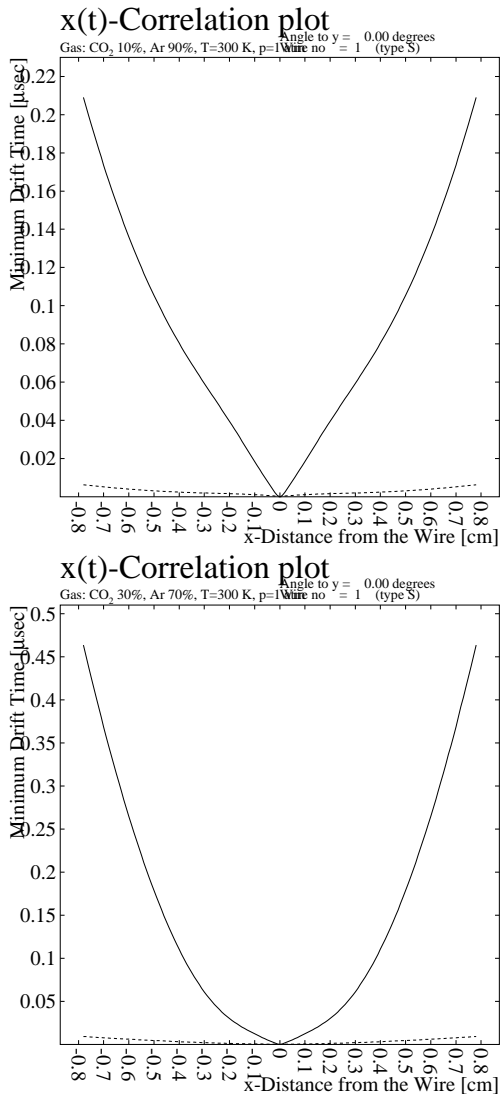
x(t)-Correlation plot

Gas: CO$_2$ 10%, Ar 90%, T=300 K, p=1 Wire no = 1   (type S)
Angle to y = 0.00 degrees

Minimum Drift Time [μsec]

x-Distance from the Wire [cm]

x(t)-Correlation plot

Gas: CO$_2$ 30%, Ar 70%, T=300 K, p=1 Wire no = 1   (type S)
Angle to y = 0.00 degrees

Minimum Drift Time [μsec]

x-Distance from the Wire [cm]

FIG. 19: Drift-to-distance relationship for two gas mixtures with no external magnetic field applied. Left: 90%-10% argon-CO$_2$ (1450 V on the wires); right: 70%-30% argon-CO$_2$ (1750 V on the wires).

the same) is identified as the actual track and passed to the track fitting algorithm.

2. Track fitting

At this stage, the distances between the found track in the x-y plane (plane perpendicular to the axial wires) with equation: $Ax+By+1=0$ and the hit-radii are minimized using MINUIT [40]. This software package finds the values for A and B which minimizes the function:

$$\sum_{i=1}^{\#hits} \left[\frac{r_{hit}(i)^2 - \frac{(Ax_0(i)+By_0(i)+1)^2}{A^2+B^2}}{\sigma_{hit}(i)} \right]^2 . \qquad (4)$$

#

Residuals of straw 7 [μm] (Drift distance: 5-6 mm)

#

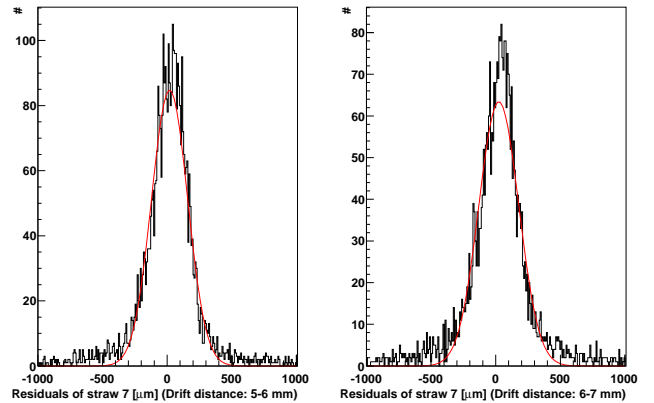Residuals of straw 7 [μm] (Drift distance: 6-7 mm)

FIG. 20: Two examples of residual histograms. The red line indicates the result of a Gaussian fit.

The numerator is the difference between the hit radius squared (r_{hit}^2) and the distance between the found track and the center of the straw squared ($\frac{(Ax_0+By_0+1)^2}{A^2+B^2}$), with ($x_0,y_0$) the coordinates of the center of the straw. The error on the hit radius, σ_{hit}, is set to a constant and does not have an influence on the minimization.

3. No external magnetic field

The position resolution is calculated for wire 7 for different gas mixtures as a function of the straw radius. This wire was chosen because of its central location. This calculation is done by selecting tracks with at least 5 hits and performing track fitting on them with wire 7 left out. The distance between the hit-radii of wire 7 and the fit tracks (also called residuals) are put into histograms. Examples of residual histograms can be seen in Fig. 20. This plot is fit with a Gaussian and the width of the Gaussian is quoted as the resolution.

The data are compared to MC simulations and shown in Fig. 21. It is readily recognized that the resolution depends on the amount of CO$_2$ in the gas mixture. This is due to overall drift times increasing with the amount of CO$_2$ increases. For short drift distances the resolution tends to be worse because the slope in the time-to-distance relation is shallower at drift distances smaller than 3 mm (see Fig. 19). Generally the MC simulation describes the data very well. This supports the use of the MC to study the effect of an external magnetic field on the position resolution of the detector.

At very small drift distances the resolution degrades due to discrete ionization statistics close to the wire: the ionization can happen right next to the wire or a little bit above or below it. When the closest ionization does not happen next to the wire the extracted drift radii are too big and this effect causes degrading resolutions.
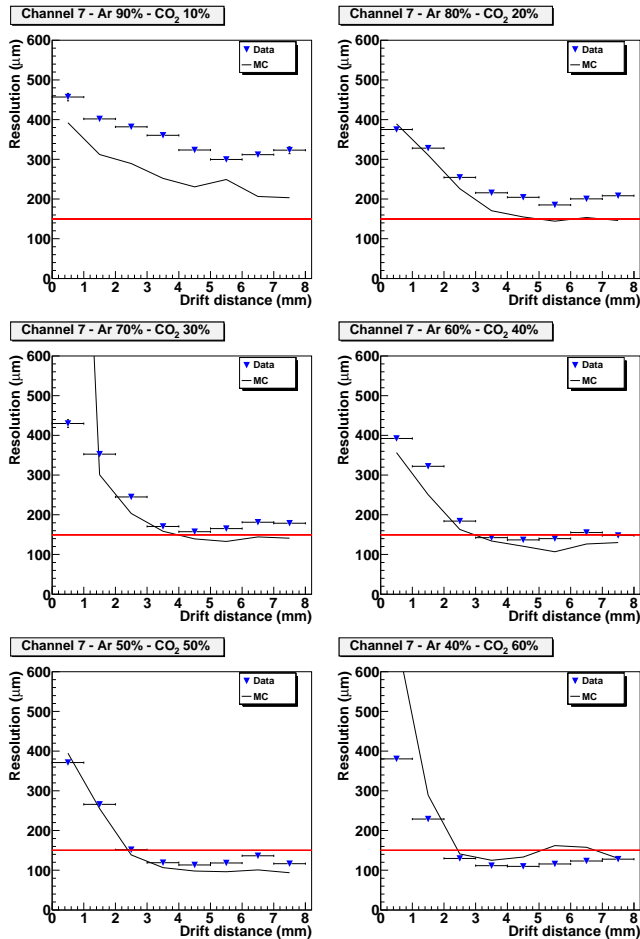
FIG. 21: Position resolutions as a function of drift distances obtained using different argon-CO_2 mixtures with no external magnetic field present. Both Monte Carlo and data results are shown. The red line indicates the design resolution.

4. External magnetic field

A parameter that changes due to an external magnetic field is the maximum drift time. The longest possible drift times with and without an external magnetic field are shown in Table IV. Drift times shorter than 1 μs are desired to avoid pile up. All gas mixtures satisfy this requirement, although the 40%-60% argon-CO_2 mixture comes close to that limit.

To examine the position resolution at a magnetic field of 2.24 T provided by the GlueX detector, a MC simulation is used. The results for different gas mixtures are shown in Fig. 22. One can observe the same general behavior as without an external magnetic field but the resolution is improved overall (around 150 μm) and meets the specifications defined in [2] for drift distances longer than 2 mm.

These tests show that gas mixtures between 60%-40% and 40%-60% argon-CO_2 satisfy the requirements outlined in the introduction and can therefore be used in the final setup in Hall-D. It is advantageous for safety con-
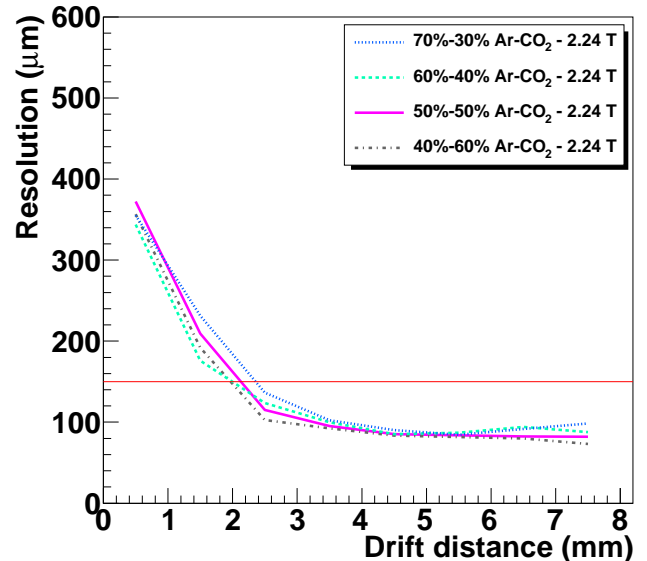

FIG. 22: Position resolution as a function of drift distance obtained using a Monte Carlo simulation with different argon-CO_2 mixtures and a 2.24 T external magnetic field. The red line indicates the design resolution.

siderations that the required resolution can be achieved without including a flammable gas component.

E. Efficiency

The efficiency of a given straw is calculated by dividing the number of tracks with five (or more) hits that go through the given straw by the number of tracks with four (or more) hits (given straw excluded) that are expected to go through the given straw. The efficiency of straw 7 as a function of drift distance is shown in Fig. 23. It is close to 100% but degrades close to the edge of the straw where the track length inside the straw is very short, this can be seen in in Fig. 15: long drift-times mean large drift-circles and short track lengths inside the straw. However, the close-pack design of the CDC will ensure high efficiency for hits in adjacent layers.

VIII. ENERGY LOSS STUDIES

Firstly, the energy loss is studied as a function of incident angle. In order to do this the detector needed to be tilted. The tilt angle is reconstructed from the energy loss. The primary motivation of this study is to see if the tilted detector behaves as expected, because in earlier prototypes deviations were observed that lead back to gas leaks, sagging of the straw, etc. Secondly, the energy loss as a means of identifying low momentum particles is investigated.
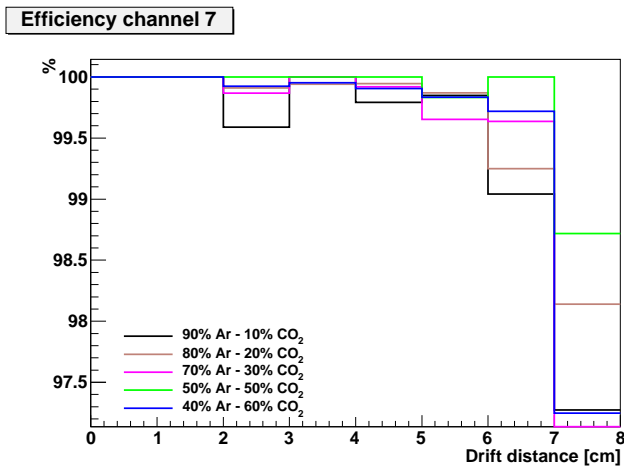
FIG. 23: Efficiency of straw 7 as a function of drift distance for several gas mixtures.

FIG. 24: Reconstructed angle of the tilted chamber as a function of straw number. See text for more details.

A. Tilted chamber

In order to increase the average incident angle of the cosmic rays with respect to the test chamber, the chamber was tilted as indicated in the top of Fig. 14. In such a configuration the average path length of cosmic rays inside the straw becomes longer and the average energy deposition larger. The chamber was positioned at two different angles: 35 and 45 degrees (see Fig. 14). A 90%-10% argon-CO_2 gas mixture was used in the 35 degree setup and a 70%-30% argon-CO_2 mixture in the 45 degree setup. The average energy deposition was measured and compared with the results obtained with the chamber in the horizontal position (see Fig. 14). As a result the measured energy deposition can be used to reconstruct the angle θ_{rec} to which the chamber was tilted using following relation:

$$\theta_{rec} = \cos^{-1}\left(\frac{\langle E_0 \rangle \cdot 0.92}{\langle E_\theta \rangle}\right). \qquad (5)$$

E_0 is the energy deposition with the detector in horizontal position and E_θ the energy deposition with the detector tilted at the angle θ. Only the energy deposition of fully reconstructed tracks was used. The factor 0.92 is the solid angle correction to the trigger counters, which systematically moves the average track angle with the chamber in its horizontal position. In Fig. 24, one can see the reconstructed angle as a function of channel number (see Fig. 15). The angles can be accurately reconstructed.

B. Particle identification

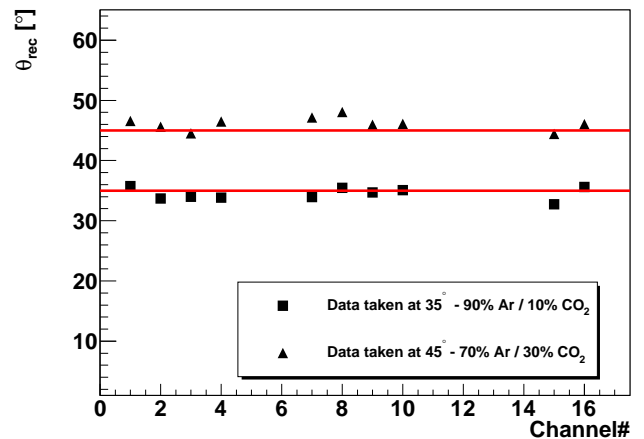In order to determine the effectiveness of this chamber to identify pions, kaons, and protons using energy loss (dE/dx), a MC study based on the realistic simulation described previously was undertaken. There is no intention to give a complete description of Particle IDentification (PID) here, but rather to investigate the principle. Pions, kaons, and protons were generated using the MC described in section VI B. The dE/dx or energy (E) loss per unit of length (x) distribution in one straw is calculated. An example of a dE/dx distribution in one straw (one layer) is shown in Fig. 25). A toy MC is used to generate energy losses according to the extracted distributions. In this way energy losses of multiple hits (or layers) can be combined to improve PID possibilities. When multiple layers are combined, the hit with the largest dE/dx and the hit with the lowest dE/dx are removed. This is an empirical method to make the Landau tails shorter and improve the separation of particles. However, in this case this method only slightly improves PID possibilities.

1. 350 MeV Pions, kaons, and protons

In Fig. 25 the simulated energy loss in one straw of pions, kaons, and protons with momenta of 350 MeV is shown. The expected Landau shaped curve is observed. Fig. 26 shows the dE/dx distributions of pions, kaons, and protons with a momentum of 350 MeV for 14 and 28 layers combined. A reasonable separation between pions and protons can be achieved, while it will be difficult to distinguish kaons from pions for example. This PID information can be included in a kinematic fit to identify the most likely particle type for a given track.

2. 250 MeV Pions and kaons

Fig. 27 shows the energy loss distribution in one straw of pions and kaons with a momentum of 250 MeV. Pro-
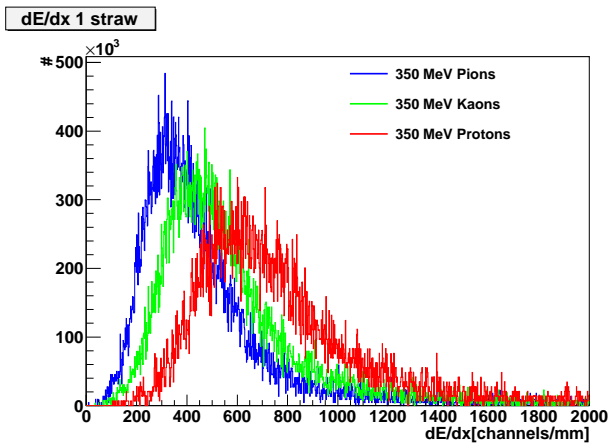
FIG. 25: Pion, kaon, and proton dE/dx distribution.
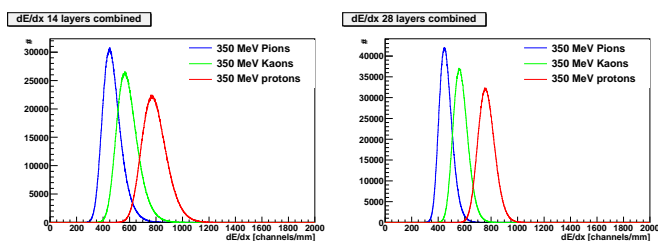
FIG. 26: Pion, kaon, and proton dE/dx distributions of several layers combined.

tons are not shown here because their momentum is not sufficient to pass through more than a few layers of straws. Fig. 28 shows the energy loss distributions of pions and kaons with a momentum of 250 MeV for several layers combined. A reasonable separation between pions and kaons is observed.
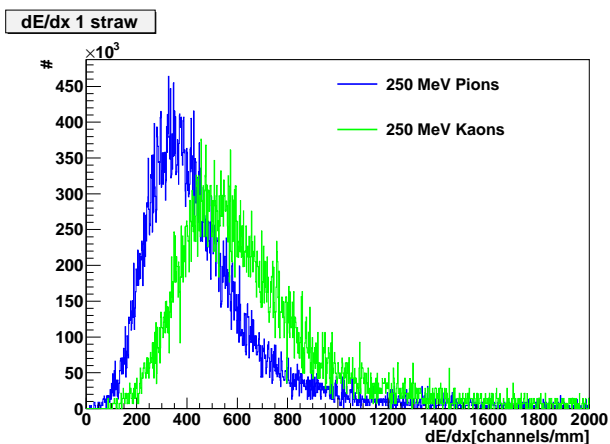
FIG. 27: Pion and kaon dE/dx distributions.
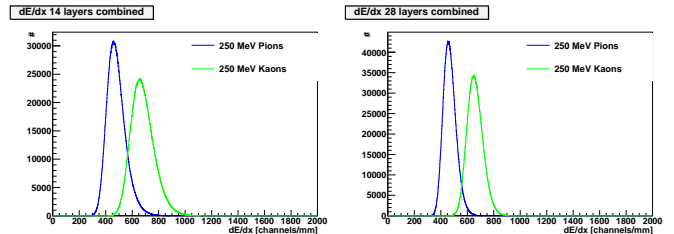
FIG. 28: Pion and kaon dE/dx distributions of several layers combined.
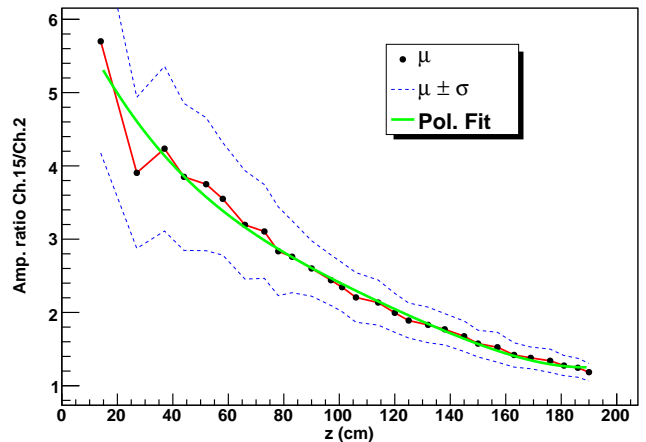
FIG. 29: Amplitude ratios of ^{55}Fe induced signals as a function of position along the wire.

IX. CHARGE DIVISION

In this study, the full-scale prototype shown in Fig. 13 is used. Charge division is established by connecting two neighboring straws with a 60 Ω resistor at the downstream (far) end of the straw. A two meter long wire has a resistance of 300 Ω. When a signal is induced on a wire the charge generated will be divided between the two connected wires. By taking the ratio of the two signal amplitudes, the position along the wire of the source of the signal can be calculated. This charge division thereby provides complementary information to that obtained from a combined analysis of stereo and axial wires.

As a proof of principle, a ^{55}Fe source was used in a test and placed on straw number 15 that was coupled to straw number 2 by a 60 Ω junction. With the source positioned at different locations along the wire the amplitudes of the signals were determined and the ratio calculated. The result is shown in Fig. 29. In the GlueX experiment, most of the signals are expected to be generated at $z > 80$ cm because of the location of the target with respect to the CDC (see introduction). In that region charge division will provide a resolution along the wire of about

10 cm. More details concerning this study can be found in ref. [41].

X. CONCLUSION

The design of the GlueX straw tube central drift chamber is described in detail. Many design parameters (straw tube material, placement of stereo straws, etc.) have been determined by comparing experimental data from prototype chambers with MC simulation. The choice of gas type and mixture at which to operate the chamber has been determined by properties such as drift-times, which are extracted using flash ADCs, and position resolution. A realistic MC simulation was developed that reproduces the experimental results. The simulation has been used to predict the expected particle identification sensitivity using energy deposition. A test of charge division by connecting neighboring wires has been conducted and shows that position resolution of about 10 cm can be achieved along the direction of the wire.

[1] C.A. Meyer and Y. Van Haarlem, **The Status of Exotic-quantum-number Mesons**, *To be submitted to Phys. Rev. C.*

[2] The GlueX collaboration, **The GlueX Experiment**, GlueX Document 346, October 2004.

[3] A.R. Dzierba, C.A. Meyer, E.S. Swanson, **The Search for QCD Exotics**, Am. Sci. 88 (2000) #5.

[4] P. Baringer *et al*, **A Drift Chamber Constructed of Aluminized Mylar Tubes**, Nucl. Instr. and Meth. A 254 (1987) 542.

[5] W.T. Ford *et al*, **Trigger Drift Chamber for the Upgraded Mark II Detector at PEP**, Nucl. Instr. and Meth. A 255 (1987) 486.

[6] W.W. Ash *et al*, **Design, Construction, Prototype Tests and Performance of a Vertex Chamber for the MAC Detector**, Nucl. Instr. and Meth. A 261 (1987) 399.

[7] S. Bhadra *et al*, **The Design and Construction of the CDF Central Drift Tube Array**, Nucl. Instr. and Meth. A 268 (1988) 92.

[8] C. Biino *et al*, **Charge Division in a small Proportional Chamber Constructed with Aluminum Mylar Tubes**, Nucl. Instr. and Meth. A 271 (1988) 417.

[9] M.T. Roman *et al*, **Readout and Trigger Electronics for the TPC Vertex Chamber**, IEEE Trans. Nucl. Sci. NS-35 (1988) 329.

[10] J. Adler *et al*, **The Mark III Vertex Chamber**, Nucl. Instr. and Meth. A 276 (1989) 42.

[11] V.M. Aulchenko *et al*, **Vertex Chamber for the KEDR detector**, Nucl. Instr. and Meth. A 283 (1989) 528.

[12] S.H. Oh *et al*, **Design and Performance of a Straw Tube Drift Chamber**, Nucl. Instr. and Meth. A 303 (1991) 277.

[13] M. Frautschi *et al*, **The AMY inner tracking chamber**, Nucl. Instr. and Meth. A 307 (1991) 52.

[14] C. Bromberg *et al*, **Design and Operation of large Straw-Tube Drift Chamber Planes**, Nucl. Instr. and Meth. A 307 (1991) 292.

[15] A. Baldin *et al*, **Proposals for a New Type of Microchannel-Plate-Bases Vertex Detector**, Nucl. Instr. and Meth. A 323 (1992) 439.

[16] N.M. Hamann *et al*, **The JETSET Barrel Drift-Tube ("Straw") Chamber**, Nucl. Instr. and Meth. A 346 (1994) 57.

[17] G. Bonvicini *et al*, **Construction and Testing of a Precision 2 m Long Straw Chamber Prototype**, Nucl. Instr. and Meth. A 359 (1995) 492.

[18] C. Brandt *et al*, **Construction and Beam Test Results for the Delphi Two Meter Straw Detector**, Nucl. Instr. and Meth. A 367 (1995) 129.

[19] S. Graessle *et al*, **A Straw Tracking System to Study rare K_L Decays**, Nucl. Instr. and Meth. A 367 (1995) 138.

[20] C. Avanzini *et al*, **High Precision Limited Streamer Drift Tubes**, Nucl. Instr. and Meth. A 367 (1995) 154.

[21] A.F. Sustavov *et al*, **Thin-Wall Drift Tube Vertex Chamber for the AMPIR Spectrometer**, Nucl. Instr. and Meth. A 367 (1995) 159.

[22] S.H. Oh *et al*, **High Rate Test of a Straw Drift Chamber**, Nucl. Instr. and Meth. A 369 (1996) 37.

[23] Y. Arai *et al*, **A Modular straw drift tube tracking system for the Solenoidal Detector Collaboration Experiment Part I. Design**, Nucl. Instr. and Meth. A 381 (1996) 355.

[24] Y. Arai *et al*, **A Modular straw drift tube tracking system for the Solenoidal Detector Collaboration Experiment Part II. Performance**, Nucl. Instr. and Meth. A 381 (1996) 372.

[25] G. Garino *et al*, **A Straw Drift Chamber for the TAGX Spectrometer**, Nucl. Instr. and Meth. A 388 (1997) 100.

[26] T.A. Armstrong *et al*, **Large Straw-Tube Tracking Chambers for AGS Experiment E864**, Nucl. Instr. and Meth. A 425 (1999) 210.

[27] C. Leonidopoulos *et al*, **Development of a Straw Tube Chamber with Pickup-Pad Readout**, Nucl. Instr. and Meth. A 427 (1999) 465.

[28] M. Ambriola for the PAMELA Collaboration, **Performance of the Transition Radiation Detector of the PAMELA Space Mission**, Nucl. Phys. B proc. suppl. 113 (2002) 322.

[29] V.N. Bychkov *et al*, **The Large Size Straw Drift Chambers of the COMPASS experiment**, Nucl. Instr. and Meth. A 556 (2006) 66.

[30] The ATLAS TRT collaboration *et al*, **The ATLAS TRT Barrel Detector**, 2008 JINST 3 P02014.

[31] C. A. Meyer, **Donut and Insert Specifications**, GlueX Document 1284, June 2009.

[32] Y. Van Haarlem, **Central Drift Chamber straw radiation test results**, GlueX Document 1379, December 2009.

[33] D. Lawrence, **M.C. Studies of CDC Axial/Stereo layer configuration**, GlueX Document 1191, January 2009.

[34] C. A. Meyer, **CDC Gas Flow**, GlueX Document 1243, June 2009.

[35] F. Barbosa and D. Carman, **High Voltage Distribution for the Hall D CDC and FDC Detectors**, GlueX Document 967, February 2009.

[36] F. Barbosa, **Tests of the New GlueX Preamplifier - GAS-II & GPC-II**, GlueX Document 1364, November 2009.

[37] G. Visser, **Receiver/Shaper Prototype for FDC&CDC for use with Struck ADC's**, GlueX Document 736, January 2007.

[38] G. Visser and F. Barbosa, **fADC125 - VME64x Flash ADC Module Specifications**, GlueX Document 862, September 2007.

[39] R. Veenhof, **The GARFIELD Program, Simulation of Gaseous Detectors**, http://garfield.web.cern.ch/garfield/, 1984.

[40] F. James, **MINUIT: Function Minimization and Error Analysis, v. 94.1**, CERN Program Library D506.

[41] B. Dey, Y. Van Haarlem, C. A. Meyer, **Charge Division measurements with CDC prototype for z-position tracking in GlueX**, GlueX Document 1332, September 2009.